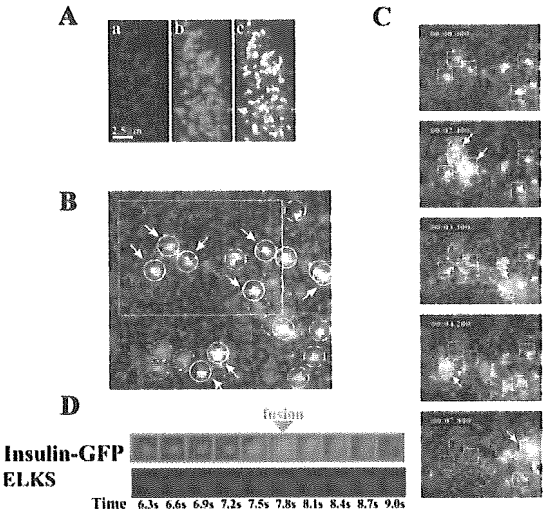

Figure 7. ELKS clusters are sites for docking and fusion of insulin granules in living cells. (A) TIRF image of ELKS in the plasma membrane labeled with TAT-conjugated Cy3-labeled anti-ELKS mAb and stained with anti-ELKS pAb. After MIN6 cells were treated with TAT-conjugated Cy3-labeled anti-ELKS mAb for 30 min, cells were fixed and immunostained with anti-ELKS pAb and then were observed with TIRFM. There was significant colocalization (c) between ELKS clusters labeled with TAT-conjugated, Cy3-labeled antibody (a) and those stained with pAb (b). (B) TIRF image of GFP-tagged insulin granules and Cy3-labeled ELKS clusters in living MIN6 cells and dual image analysis of GFP-tagged insulin granule motion at ELKS clusters during 50 mM KCl stimulation. Three days after MIN6 cells were transfected with the expression vector insulin-GFP (green), cells were treated with TAT-conjugated Cy3-labeled anti-ELKS antibody (red) for 50 min. Each circle (1 μm in diameter) in the green channel corresponds to the circle in the red channel. Solid circles represent the colocalization of insulin granules and ELKS clusters. Dotted circles indicate observed insulin granules, but not ELKS clusters. Dashed circles indicate insulin granules with only a partially corresponding overlap. Arrowed circles represent the insulin granules that eventually were fused by stimulation with 50 mM KCl (see the dual-colored movie in supplemental data). Box indicates the area in C. (C) Insulin granules underwent exocytosis at ELKS clusters. The box (1 $\times$ 1 μm) indicates the granule to be fused. Timestamp (minute:second:millisecond) was overlaid. Time 0 indicates the addition of KCl. (D) Sequential images (1 $\times$ 1 μm, 300-ms intervals) of a single insulin granule (green) at the ELKS cluster (red) during stimulation with 50 mM KCl.

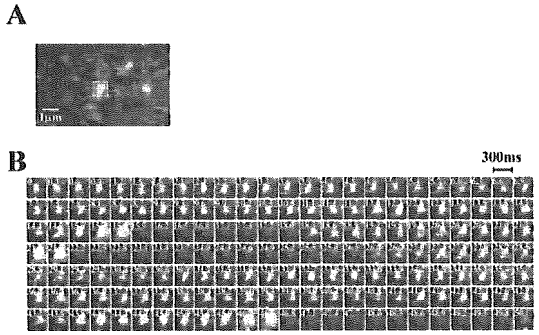

Figure 8. Repeated fusion from insulin granules on the same site of ELKS cluster. (A) Dual imaging of GFP-tagged insulin granules and Cy3-labeleld ELKS clusters in living MIN6 cells. The box indicates the granule to be fused repeatedly. (B) Sequential images analysis boxed in A (1 $\times$ 1 μm, 300-ms intervals) of repeated fusion from GFP-tagged insulin granules (green) at the same Cy3-labeled ELKS cluster (red), during 50 mM KCl stimulation. Time 0 indicates the addition of KCl. The time of each frame in the sequence is indicated in seconds.

specifically found endogenous ELKS clusters in the plasma membrane. MIN6 cells treated with TAT-conjugated, Cy3 labeled mAb for 30 min were fixed and immunostained with anti-ELKS pAb. As shown in Figure 7A, there was significant overlapping of ELKS clusters labeled with TAT-conjugated, Cy3-labeled mAb (red) and those stained with pAb (green).

To examine whether insulin fusion occurs on ELKS clusters, MIN6 cells were first transfected with GFP-tagged insulin expression vector and then were treated with TAT-conjugated, Cy3-labeled anti-ELKS mAb. Stimulation with high KCl (50 mM) showed that the fusion events of insulin granules occurred frequently at the ELKS clusters; 67.3 $\pm$ 6.7 and 16.2 $\pm$ 5.5% of all fusion events fully or partially occurred on the ELKS clusters, respectively, whereas 16.5 $\pm$ 3.6% of the fusion events occurred on sites other than ELKS clusters (n = 4 cells) (Figure 7B, granules to be fused are indicated by arrows; also see Figure 7C and Supplemented Movie 1). Thus, the data indicate that fusion frequently occurs on ELKS clusters. On the other hand, because the distribution of ELKS clusters and insulin granules is widespread, the occurrence of insulin fusion on ELKS clusters may be accidental. To address this issue, we examined three other regions that were randomly chosen. The data demonstrated that, on region 1, 62.8 $\pm$ 8.3 and 18.5 $\pm$ 4.8% of all fusion events fully or partially occurred on ELKS clusters, respectively (n = 4 cells); and on region 2, 59.8 $\pm$ 7.5 and 16.9 $\pm$ 4.9% of all fusion events fully or partially occurred on ELKS clusters, respectively (n = 4 cells); on region 3, 60.2 $\pm$ 7.5 and 15.8 $\pm$ 7.4% of the all fusion events fully or partially occurred on ELKS clusters, respectively (n = 4 cells). Thus, for all regions, we obtained the same numbers, strongly indicating that the occurrence of insulin fusion on ELKS clusters is not accidental.

Figure 7D shows sequential images (1 $\times$ 1 μm, 300-ms intervals) of a single granule (green) and an ELKS cluster (red) simultaneously observed during KCl stimulation and demonstrates that GFP-tagged insulin was diffused laterally through fusion on the plasma membrane, whereas no changes were observed in the ELKS clusters (also see Supplemental Movie 1). Because the number of fusion events in the cells transduced with TAT-conjugated mAb was similar to that in control cells, labeling endogenous ELKS with TAT-conjugated, Cy3-labeled mAb did not affect insulin exocytosis (our unpublished data).

Interestingly, we observed repeated fusion from insulin granules at the same sites on ELKS cluster (Figure 8A). In MIN6 cells, most fusion events (90% of the total fused granules) evoked by KCl stimulation occurred from previously docked granules, with ~10% of the fusion occurring from newly recruited granules (Ohara-Imaizumi *et al.*, 2002b), and the fusion events of newly recruited granules also mostly occurred on the ELKS clusters (63.1 $\pm$ 5.2 and 19.4 $\pm$ 2.9% of all fusion events fully or partially occurred on sites at the ELKS clusters, respectively, whereas 17.4 $\pm$ 3.9% of the fusion events did not occur on the ELKS clusters; n = 10 cells). The present data revealed that some of the fusion events from newly recruited granules occurred repeatedly on the same ELKS cluster (Figure 8B).

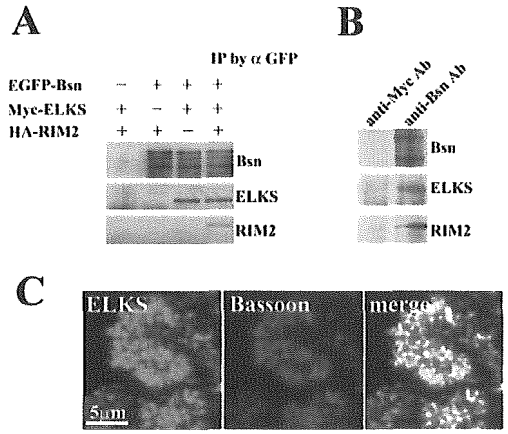

Figure 9. Interaction with ELKS and Bassoon. (A) In vitro binding studies of ternary complex formation of ELKS, Bassoon, and RIM2. Each expression plasmid of Myc-ELKS, HA-RIM2, or EGFP-Bassoon was transfected into HEK293 cells. Each protein was extracted and mixed, in the indicated combinations, followed by immunoprecipitation by using anti-GFP antibody (α GFP). Immunoprecipitates were then analyzed by immunoblotting by using the anti-GFP, anti-Myc, and anti-HA antibodies. IP, immunoprecipitation. (B) Coimmunoprecipitation assay in MIN6 cells. MIN6 cell lysates were immunoprecipitated with anti-Bassoon mAb or anti-Myc mAb (as a control). The immunoprecipitates were subjected to immunoblot analysis with anti-Bassoon mAb, anti-ELKS pAb, and anti-RIM2 pAb. Note that when Bassoon was immunoprecipitated by its antibody, ELKS and RIM2 were coimmunoprecipitated with Bassoon. (C) Colocalization of ELKS and Bassoon in the plasma membrane of MIN6 cells analyzed by TIRFM. Cells were fixed and double immunostained using anti-ELKS pAb and anti-Bassoon mAb, followed by secondary antibodies (Alexa Fluor-488–conjugated anti-rabbit and Alexa Fluor 546-conjugated antimouse antibodies). The colocalization of ELKS clusters (green) and Bassoon clusters (red) is demonstrated by the overlap (yellow) of green and red channel images.

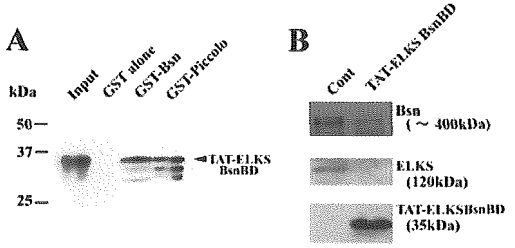

Figure 10. TAT-ELKSBsnBD binds Bassoon (A) and inhibits the binding of ELKS and Bassoon. (A) Direct binding of TAT-ELKSBsnBD to Bassoon by pull-down assay. The GST fusion proteins containing Bassoon and Piccolo as well as GST alone were immobilized to glutathione-Sepharose beads. Myc-tagged TAT-ELKSBsnBD was then incubated with the beads. Proteins that bound to the beads were analyzed by immunoblotting by using anti-Myc mAb. Arrowheads indicate TAT-ELKSBsnBD. Note that TAT-ELKSBsnBD found GST-Bassoon and GST-Piccolo, but it did not bind GST alone. (B) Effects of TAT-ELKSBsnBD on the binding of ELKS and Bassoon. Immunoprecipitation assay of Myc-ELKS and EGFP-Bassoon was performed in the presence or absence of Myc-tagged TAT-ELKSBsnBD by using anti-GFP antibody, followed by immunoblotting by using the anti-Myc and anti-GFP antibodies. Note that the binding of ELKS and Bassoon was inhibited in the presence of TAT-ELKSBsnBD.

Association of ELKS Interacting with Bassoon with the Docking and Fusion of Insulin Granules

Finally, we investigated whether ELKS is implicated in regulating the docking and fusion of insulin granules. We had previously found that the immunostaining of ELKS overlapped that of Bassoon in hippocampal neurons (Deguchi-Tawarada *et al.*, 2004). Indeed, in vitro binding studies demonstrated that ELKS binds Bassoon and RIM2 (Figure 9A). As shown in Figure 9A, when cell lysates expressing Myc-ELKS and EGFP-Bassoon and HA-RIM2 were immunoprecipitated with anti-GFP antibody, ELKS was coimmunoprecipitated in the presence or absence of RIM2, whereas RIM2 was coimmunoprecipitated only in the presence of ELKS. These results demonstrate that ELKS forms a ternary complex with Bassoon and RIM2, thus indicating that ELKS function is associated with these CAZ-related molecules. Indeed, in MIN6 cells, when Bassoon was immunoprecipitated by its antibody, ELKS and RIM2 were coimmunoprecipitated with Bassoon, indicating that ELKS forms a ternary complex with Bassoon and RIM2 (Figure 9B). In addition, TIRF imaging of dual immunostaining for ELKS and Bassoon clearly showed that most ELKS clusters were colocalized with Bassoon in the plasma membrane (Figure 9C).

We, therefore, analyzed insulin granule docking and fusion when the action of ELKS was inhibited by the transduction of the ELKS Bassoon-binding domain peptide. We produced both a Bassoon-binding domain of ELKS (aa 405–602) fused to a TAT peptide (TAT-ELKSBsnBD) and a non-coiled-coil domain of ELKS (aa 324–403) fused to a TAT peptide, as the control (TAT-ELKSContD), and then transduced either ELKSBsnBD or ELKSContD into MIN6 cells by means of the TAT system, as described previously (Ohara-Imaizumi *et al.*, 2002a). We first examined, by pull-down assay, whether TAT-ELKSBsnBD binds Bassoon. As shown in Figure 10A, TAT-ELKSBsnBD binds GST-Bassoon but does not bind GST alone. The TAT-ELKSBsnBD also binds GST-Piccolo, which is structurally related to Bassoon and binds the Bassoon binding region of CAST (Takao-Rikitsu *et al.*, 2004). Next, to examine the effects of TAT-ELKSBsnBD on the binding of ELKS and Bassoon, we performed an immunoprecipitation assay for Myc-ELKS and EGFP-Bassoon in the presence or absence of TAT-ELKSBsnBD. As shown in Figure 10B, TAT-ELKSBsnBD inhibited the binding of Bassoon to ELKS, indicating that TAT-ELKSBsnBD can disrupt the formation of the ELKS and Bassoon complex.

We then monitored the docking and fusion process of GFP-tagged insulin granules in TAT-ELKSBsnBD–treated MIN6 cells stimulated by 22 mM glucose. TAT-ELKSBsnBD was quickly delivered into the MIN6 cells in <30 min (Figure 11A). As shown in the histogram of the number of fusion events per minute (Figure 11B, control), the fusing granules originated mostly from previously docked granules (Figure 11B, red column) during the first phase of glucose-stimulated insulin release (0–4 min), whereas during the second phase (>4 min) those fusion granules arose mostly from newly recruited granules (Figure 11B, green column), as described previously (Ohara-Imaizumi *et al.*, 2002a,b). TAT-ELKSBsnBD treatment not only reduced the fusion events during the first phase of release but also strongly inhibited the second phase of release, whereas TAT-ELKSContD treatment had no effect on either phase, indicating that the effect of TAT-ELKSBsnBD is specific. During the first phase, TAT-ELKSBsnBD treatment reduced the total number of fusion events, which mostly arose from previously docked granules, to ~59% that of control levels (20.4 ± 1.0 in TAT-ELKSContD–treated cells vs. 12.1 ± 0.4 in TAT-ELKSBsnBD–treated cells, $n = 10$, $p < 0.005$). In contrast, fusion events in the second phase of insulin release mostly oc-

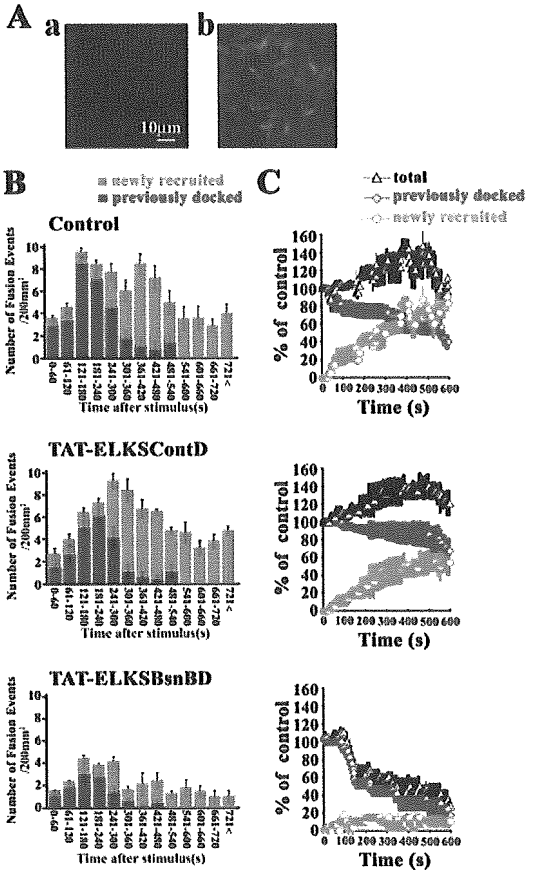

Figure 11. TAT-ELKSBsnBD inhibits both phases of insulin release. (A) Transduction of TAT-ELKSBsnBD into MIN6 cells. Control cells (a) and Myc-tagged TAT-ELKSBsnBD-treated (70 μg/ml for 50 min) cells (b) were fixed, immunostained for Myc, and deserved by confocal laser-scanning microscopy. (B) Analysis of fusion events of GFP-tagged insulin granules in control, TAT-ELKSContD-treated, and TAT-ELKSBsnBD–treated MIN6 cells by high-glucose (22 mM) stimulation with TIRFM. MIN6 cells expressing GFP-tagged insulin were treated with and/or without 70 μg/ml TAT fusion protein for 50 min, and TIRF images were acquired every 300 ms by 22 mM glucose stimulation. The fusion events (200 μm^2) were manually counted as described in *Materials and Methods*. The histogram shows the number of fusion events (n = 6 cells) at 1-min intervals after high glucose (22 mM) stimulation in control and the TAT fusion protein-treated cells. The histogram is divided into two categories: fusion from previously docked granules (red column) and newly recruited docked granules (green column). Data are mean ± SEM. (C) Time-dependent change of the number of insulin granules docked to the plasma membrane. The number of previously docked granules (red line) and the number of newly recruited granules (green line) during 22 mM glucose stimulation were determined by counting granules on each sequential image (200 μm^2, n = 3 cells each) in control and in TAT fusion protein-treated cells. Black line shows the total number of docked granules and corresponds to the sum of the red and green lines. Time 0 indicates the addition of high glucose (22 mM). The number of previously docked granules at time 0 was taken as 100% (46, 55, and 65 granules, respectively, in each of the control cells; 49, 59, and 57 granules, respectively, in each of the TAT-ELKSContD-treated cells; 52, 57, and 68 granules, respectively, in each of the TAT-ELKSBsnBD-treated cells). Data are mean ± SEM.

curred from newly recruited docked granules and were markedly inhibited (to ~32% of control levels) by TAT-ELKSBsnBD treatment (52.2 ± 2.0 in TAT-ELKSContD–

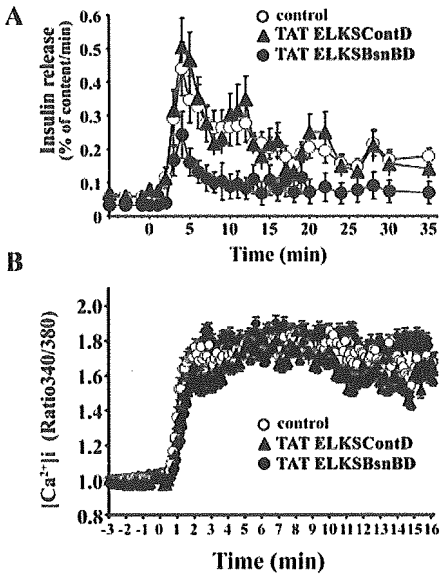

Figure 12. Effects of TAT-ELKSBsnBD on insulin release and on $[Ca^{2+}]_i$ response to high glucose in MIN6 cells. (A) Insulin release from perifused control and the TAT fusion protein-treated (70 μg/ml for 50 min) cells stimulated with 22 mM glucose. The cells in the cell chamber (~10^6 cells per chamber) were perifused with KRB (0.5 ml/min) at 37°C, and the perfusate was analyzed for IRI by radioimmunoassay. Results are given as a percentage of the cellular insulin content (2.9 $\mu g/10^6$ cells in control cells, 3.1 $\mu g/10^6$ cells in TAT-ELKSContD-treated cells, and 2.8 $\mu g/10^6$ cells in TAT-ELKS-BsnBD–treated cells). (B) Glucose-induced changes in $[Ca^{2+}]_i$ in control and the TAT fusion protein-treated (70 μg/ml for 50 min) cells. Glucose-induced changes in $[Ca^{2+}]_i$ were measured in each treated cells by Fura-2 AM (5 μM). Time 0 indicates the time of the addition of high glucose. The fluorescence ratio (340/360) at time 0 was taken as 1.

treated cells vs. 16.7 ± 1.6 in TAT-ELKSBsnBD–treated cells, n = 10, $p < 0.0005$). These results were consistent with the data for endogenous insulin release from perifused cells treated with TAT-ELKSBsnBD (Figure 12A). The dynamic changes in the total number of docked granules during glucose stimulation in TAT-ELKSBsnBD–treated cells showed that the total number of docked granules during the time course decreased because the number of newly recruited granules to eventually dock to the plasma membrane did not increase (Figure 11C). On the other hand, as was observed in TAT-ELKSContD–treated cells, TAT-ELKSB-snBD did not alter the glucose-induced change in intracellular Ca^{2+} concentration $[Ca^{2+}]_i$ measured by loading cells with Fura-2 AM (Figure 12B). These findings suggest that ELKS together with Bassoon is involved in the docking and fusion of insulin granules.

Silencing of ELKS with Specific siRNA Attenuates Glucose-evoked Insulin Release from MIN6 β Cells

We further examined whether ELKS clusters are required for insulin exocytosis by silencing ELKS with siRNA technology. One of the double-stranded RNA oligos was designed according to the mouse ELKS cDNA sequence (ELKS siRNA) and delivered to the MIN6 cells by transient transfection, as described in *Materials and Methods*. First, we studied how ELKS siRNA works by using HEK293 cells. As shown in Figure 13A, the ELKS silencer strongly suppressed

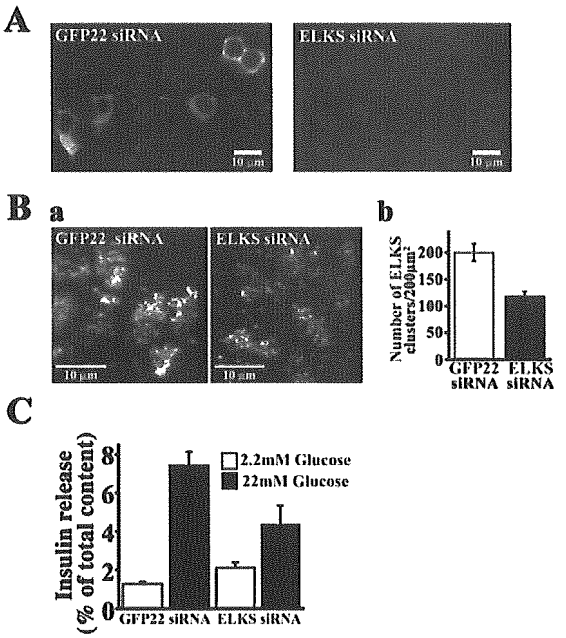

Figure 13. Silencing ELKS in MIN6 cells with RNAi. (A) ELKS siRNA suppressed expression of recombinant Myc-tagged ELKS in HEK293 cells. The expression vector encoding Myc-tagged ELKS and GFP-22 siRNA (as control) or ELKS siRNA were cotransfected into HEK293 cells. Two days after transfection, cells were fixed, permeabilized, and stained with anti-Myc mAb and Alexa Fluor-546–conjugated anti-mouse secondary antibody. The fluorescence image was analyzed by confocal laser scanning microscopy. Note that ELKS siRNA efficiently silenced the expression of Myc-tagged ELKS. (B) a, silencing of endogenous ELKS in MIN6 cells with siRNA caused reduction of number of ELKS clusters. GFP-22 siRNA (as control) or ELKS siRNA was transfected into MIN6 cells. At 3 d after transfection, cells were fixed, permeabilized, and stained with anti-ELKS pAb and Alexa Fluor-546–conjugated anti-rabbit secondary antibody. The fluorescence image was analyzed by TIRFM. Note that the number of ELKS clusters was markedly reduced on the plasma membrane of ELKS siRNA-transfected cells, compared with GFP-22 siRNA-transfected cells. b, number of ELKS clusters in the plasma membrane. The number of individual fluorescent spots of ELKS shown in TIRF images was counted. Data are mean ± SE for each transfected cell (n = 40 cells each). (C) Silencing of endogenous ELKS with siRNA caused a decrease of glucose-evoked insulin release from MIN6 cells. GFP-22 (control) or ELKS siRNA-transfected MIN6 cells were incubated for 15 min with basal low glucose (2.2 mM) or high glucose (22 mM). Data are mean ± SEM of eight determinations from individual wells.

expression of recombinant Myc-tagged ELKS when the expression vector encoding Myc-tagged ELKS (full length, aa 1–948) and ELKS siRNA were cotransfected into HEK293 cells. The GFP-22 siRNA, used as noninterfering control, had no effect on ELKS expression. Thus, our designed ELKS siRNA was found to be effective for inhibiting ELKS RNA expression. Then, ELKS siRNA was transfected into MIN6 cells, and the number of ELKS clusters observed by TIRFM was markedly reduced, to ~60%, on the plasma membrane of the cells, compared with GFP-22 siRNA-transfected control cells. We then investigated the effect of glucose-stimulated insulin release from MIN6 cells, in which ELKS RNA expression is inhibited. The silencing of ELKS did not affect the basal release (2.2 mM glucose), but it resulted in a decrease in glucose (22 mM)-evoked insulin release, to ~58% of the release from GFP-22–transfected control cells (Figure 13C), indicating that ELKS is involved in regulated insulin release.

DISCUSSION

CAST is a novel CAZ protein (Ohtsuka *et al.*, 2002) that is associated with the active zone of neurons. CAST, also known as ERC2 (Wang *et al.*, 2002), which is mainly expressed in the brain, may serve as a key component of the CAZ structure through binding with other CAZ proteins such as Bassoon, RIM1, and Munc13-1 (Takao-Rikitsu *et al.*, 2004). ELKS, which is highly homologous to CAST, corresponds to Rab6-interacting protein 2 (Monier *et al.*, 2002), ERC1 (Wang *et al.*, 2002), and CAST2 (Deguchi-Tawarada *et al.*, 2004) and is distributed in several tissues. ELKS has been identified as a gene fused to RET tyrosine kinase in thyroid carcinomas (Nakata *et al.*, 1999; Nakata *et al.*, 2002) and may serve a regulatory function in the nuclear factor-κB activation (Ducut Sigala *et al.*, 2004); Rab6-interacting protein 2 was identified as a Rab6 small G protein-interacting protein and is likely to function in endosomes of the Golgi transport in several tissues (Janoueix-Lerosey *et al.*,1995; Monier *et al.*, 2002). Of note, ELKS was recently identified as a component of the CAZ structure in the brain that binds RIMs (Wang *et al.*, 2002; Deguchi-Tawarada *et al.*, 2004). In pancreatic β cells, the presence of an active zone for insulin exocytosis has not been found although the expression of CAZ-related proteins was reported recently (Fujimoto *et al.*, 2002). Detailed examinations of the functional roles of these proteins in insulin exocytosis are still needed, and active zones in pancreatic β cells are very attractive focus of study. In the present study, we explored the localization and function of ELKS in pancreatic β cells, and the data obtained indicate that ELKS functions in insulin exocytosis.

Immunohistochemical studies, including immunoelectron microscopic analysis, clearly revealed that ELKS was colocalized with insulin granules at the plasma membrane of β cells facing blood capillaries. Interestingly, insulin immunostaining was observed to be denser on the capillary side (Figure 1). In contrast, the immunostaining pattern of t-SNAREs (syntaxin 1 and SNAP-25), which are part of the exocytotic machinery (Daniel *et al.*, 1999; Nagamatsu *et al.*, 1999), was uniform (Sadoul *et al.*, 1995; Nagamatsu *et al.*, 1996). Thus, it is possible that ELKS may have a specialized role in leading the insulin granules to the capillary side. Indeed, Orci *et al.* (1987) reported that insulin may be released into capillaries. Thus, ELKS may have a potential role in the translocation of insulin granules to a specialized exocytotic site, such as a hot spot, observed in neuron. To correctly address this issue, observation of insulin exocytosis from islets in situ may be the best method: however, technical difficulties prevented us from using the method in the study. Nevertheless, in the present study, use of TIRFM and immunoelectron microscopy supported the idea that ELKS may have a role in forming active zone-like regions in β cells.

To study this subject in more detail, we used insulin-producing clonal cells, MIN6 cells. The data showed a regional distribution of ELKS in the plasma membrane, compared with syntaxin 1, which was uniformly distributed on the entire plasma membrane. Of note, 80% of all ELKS clusters were colocalized with insulin granules, despite the patchy distribution of ELKS in the plasma membrane, and fusion occurred on ELKS clusters, which indicates that insulin granules selectively docked to the sites of ELKS clusters. Thus, it seems that ELKS defines the fusion site of

insulin granules. In addition, we previously reported that fusion from insulin granules occurred on syntaxin 1 clusters (Ohara-Imaizumi *et al.*, 2004a); thus, we examined the triple colocalization of ELKS, syntaxin 1, and insulin granules. We observed that ~50% of insulin granules were present on the ELKS sites colocalizing with syntaxin 1 clusters. Thus, fusion was assumed to occur on these sites, which indicated that ELKS contributes to defining the fusion site. Judging from the correct definition of the active zone in neurons, which is characterized by the presence of an electron-dense matrix of cytoskeletal filaments beneath the plasma membrane where it is associated with synaptic vesicles (Landis *et al.*, 1988; Hirokawa *et al.*, 1989; Burns and Augustine, 1995), it is difficult to conclude that β cells have such an active zone. Nonetheless, the evidence that 1) ELKS is dense in the plasma membrane facing blood capillaries and that 2) fusion from insulin granules repeatedly occurs on ELKS clusters suggests the existence of an active zone in β cells. Of course, more experiments will be required to confirm our hypothesis.

Does ELKS function in insulin exocytosis? By using a TAT fusion protein, we examined whether ELKS and its interacting molecules function in the insulin exocytosis process. ELKS directly binds Bassoon and RIM2 (Figure 9A), which indicates that the function of ELKS is associated with these CAZ proteins, although the functional role of bassoon in pancreatic β cells is not known. It has been reported that CAST binds to Bassoon through the central region (second coiled-coil domain) of CAST. The microinjected Bassoon binding domain of CAST impairs synaptic transmission in cultured superior cervical ganglion neurons, which suggests that CAST regulates transmitter release in cooperation with Bassoon at the CAZ (Takao-Rikitsu *et al.*, 2004). By reference to these experiments, we speculated that ELKS may function in association with CAZ protein in insulin exocytosis; therefore, we introduced the Bassoon-binding domain of ELKS fused to TAT (TAT-ELKSBsnBD) into MIN6 cells. In TAT-ELKSBsnBD-treated cells, fusions from the previously and newly docked granules were inhibited in both the first and second phases of insulin exocytosis, in which we also observed a marked reduction in the accumulation of newly docked granules. So far, there have been no reports showing that ELKS and Bassoon are associated with syntaxin 1 and SNAP25, so that, at present, we cannot determine how CAZ proteins directly interact with SNARE proteins: nevertheless, our results suggest that ELKS, through binding to Bassoon, regulates both the docking and fusion steps in insulin exocytosis. Finally, to directly address the question of whether ELKS functions in insulin exocytosis, we performed siRNA-based experiments. The attenuation of ELKS expression by RNA interference decreased the number of ELKS clusters in the plasma membrane and reduced glucose-evoked insulin release from clonal β cells (Figure 13). Although these data are not shown, these cells showed the reduced number of docked granules. Together, our data strongly indicate that CAZ-related protein play an important role in the docking/fusion of insulin granules and may form an active zone-like region in pancreatic β cells.

In conclusion, ELKS is a possible candidate for definition of the fusion site of insulin exocytosis, and it regulates docking and fusion of insulin granules.

ACKNOWLEDGMENTS

This work was supported by Grants-in-Aid for Scientific Research (C) 17590277 (to M.O.-I.), (B) 15390108 (to S. N.), Scientific Research on Priority Areas 16044240 (to M.O.-I.), and Exploratory Research 14657043 (to S. N.) from the Japanese Ministry of Education; Culture, Sports, Science and Technology and by a grant from Japan Private School Promotion Foundation (to S. N.).

REFERENCES

Akimoto, Y., Kreppel, L. K., Hirano, H., and Hart, G. W. (1999). Localization of the O-linked N-acetylglucosamine transferase in rat pancreas. Diabetes *48*, 2407–2413.

Altrock, W. D., *et al.* (2003). Functional inactivation of a fraction of excitatory synapses in mice deficient for the active zone protein bassoon. Neuron *37*, 787–800.

Betz, A., Thakur, P., Junge, H. J., Ashery, U., Rhee, J. S., Scheuss, V., Rosenmund, C., Rettig, J., and Brose, N. (2001). Functional interaction of the active zone proteins Munc13–1 and RIM1 in synaptic vesicle priming. Neuron *30*, 183–196.

Brose, N., Rosenmond, C., and Rettig, J. (2000). Regulation of transmitter release by Unc-13 and its homologues. Curr. Opin. Neurobiol. *10*, 303–311.

Burns, M. E., and Augustine., G. J. (1995). Synaptic structure and function: dynamic organization yields architectural precision. Cell *83*, 187–194.

Castillo, P. E., Schoch, S., Schmitz, F., Sudhof, T. C., and Malenka, R. C. (2002). RIM1alpha is required for presynaptic long-term potentiation. Nature *415*, 327–330.

Daniel, S., Noda, M., Straub, S. G., and Sharp, G.W.G. (1999). Identification of the docked granule pool responsible for the first phase of glucose-stimulated insulin secretion. Diabetes *48*, 1686–1690.

Dean, P. M. (1973). Ultrastructural morphometry of the pancreatic-cell. Diabetologia *9*, 115–119.

Deguchi-Tawarada, M., Inoue, E., Takao-Rikitsu, E., Inoue, M., Ohtsuka, T., and Takai, Y. (2004). CAST 2, identification and characterization of a protein structurally related to the presynaptic cytomatrix protein CAST. Genes Cells *9*, 15–23.

Dick, O., tom Dieck, S., Altrock, W. D., Ammermüller, J., Weiler, R., Garner, C. C., Gundelfinger, E. D., and Brandstätter. J. H. (2003). The presynaptic active zone protein Bassoon is essential for photoreceptor ribbon synapse formation in the retina. Neuron *37*, 775–786.

Ducut Sigala, J. L., Bottero, V., Young, D. B., Shevchenko, A., Mercurio, F., and Verma, I. M. (2004). Activation of transcription factor NF-kappaB requires ELKS, an IkappaB kinase regulatory subunit. Science *304*, 1963–1967.

Fujimoto, K., Shibasaki, T., Yokoi, N., Kashima, Y., Matsumoto, M., Sasaki, T., Tajima, N., Iwanaga, T., and Seino, S. (2002). Piccolo, a Ca^{2+} sensor in pancreatic β-cells. J. Biol. Chem. *277*, 50497–50502.

Garcia, E. P., McPherson, P. S., Chilcote, T. J., Takei, K., and De Camilli, P. (1995). rbSec1A and B colocalize with syntaxin 1 and SNAP-25 throughout the axon, but are not in a stable complex with syntaxin. J. Cell Biol. *129*, 105–120.

Garner, C. C., Kindler, S., and Gundelfinger, E. D. (2000). Molecular determinants of presynaptic active zones. Curr. Opin. Neurobiol. *10*, 321–327.

Gundelfinger, E. D., Kessel, M. M., and Qualmann, B. (2003). Temporal and spatial coordination of exocytosis and endocytosis. Nat. Rev. Mol. Cell Biol. *4*, 127–139.

Hirokawa, N., Sobue, K., Kanda, K., Harada, A., and Yorifuji. H. (1989). The cytoskeletal architecture of the presynaptic terminal and molecular structure of synapsin 1. J. Cell Biol. *108*, 111–126.

Janoueix-Lerosey, I., Jollivet, F., Camonis, J., Marche, P. N., and Goud, B. (1995). Two-hybrid system screen with the small GTP-binding protein Rab6. Identification of a novel mouse GDP dissociation inhibitor isoform and two other potential partners of Rab6. J. Biol. Chem. *270*, 14801–14808.

Lampugnani, M. G., Resnati, M., Raiteri, M., Pigott, R., Pisacane, A., Houen, G., Ruco, L. P., and Dejana, E. (1992). A novel endothelial-specific membrane protein is a marker of Cell-Cell contacts. J. Cell Biol. *118*, 1511–1522.

Landis, D.M.D., Hall, A. K., Weinstein, L. A., and Reese, T. S. (1988). The organization of cytoplasm at the presynaptic active zone of a central nervous system synapse. Neuron *1*, 201–209.

Martin, T. F. (2002). Prime movers of synaptic vesicle exocytosis. Neuron *34*, 9–12.

Miyazaki, J., Araki, K., Yamato, E., Ikegami, H., Asano, T., Shibasaki, Y., Oka, Y., and Yamamura, K. (1990). Establishment of a pancreatic beta cell line that retains glucose-inducible insulin secretion: special reference to expression of glucose transporter isoforms. Endocrinology *127*, 126–132.

Monier, S., Jollivet, F., Janoueix-Lerosey, I., Johannes, L., and Goud, B. (2002). Characterization of novel Rab6-interacting proteins involved in endosome-to-TGN transport. Traffic *3*, 289–297.

Nakata, T., Kitamura, Y., Shimizu, K., Tanaka, S., Fujimori, M., Yokoyama, S., Ito, K., and Emi, M. (1999). Fusion of a novel gene, ELKS, to RET due to translocation t(10;12)(q11;p13) in a papillary thyroid carcinoma. Genes Chromosomes Cancer *25*, 97–103.

Nakata, T., Yokota, T., Emi, M., and Minami, S. (2002). Differential expression of multiple isoforms of the *ELKS* mRNAs involved in a papillary thyroid carcinoma. Genes Chromosomes Cancer *355*, 30–37.

Nagamatsu, S., Fujiwara, T., Nakamichi, Y., Watanabe, T., Katahira, H., Sawa, H., and Akagawa, K. (1996). Expression and functional role of syntax in 1/HPC-1 in pancreatic beta cells. Syntaxin 1A, but not 1B, plays a negative role in regulatory insulin release pathway. J. Biol. Chem. *271*, 1160–1165.

Nagamatsu, S., Watanabe, T., Nakamichi, Y., Yamamura, C., Tsuzuki, K., and Matsushima, S. (1999). Alpha-soluble N-ethlmaleimide-sensitive factor attachment protein is expressed in pancreatic beta cells and functions in insulin but not gamma-aminobutyric acid secretion. J. Biol. Chem. *274*, 8053–8060.

Ohara-Imaizumi, M., Nakamichi, Y., Nishiwaki, C., and Nagamatsu, S. (2002a). Transduction of MIN6 beta cells with TAT-syntaxin SNARE motif inhibits insulin exocytosis in biphasic insulin release in a distinct mechanism analyzed by evanescent wave microscopy. J. Biol. Chem. *277*, 50805–50811.

Ohara-Imaizumi, M., Nakamichi, Y., Tanaka, T., Ishida, H., and Nagamatsu, S. (2002b). Imaging exocytosis of single insulin secretory granules with evanescent wave microscopy: distinct behavior of granule motion in biphasic insulin release. J. Biol. Chem. *277*, 3805–3808.

Ohara-Imaizumi, M., Nishiwaki, C., Kikuta, T., Kumakura, K., Nakamichi, Y., and Nagamatsu, S. (2004a). Site of docking and fusion of insulin secretory granules in live MIN6 beta cells analyzed by TAT-conjugated anti-syntaxin 1 antibody and total internal reflection fluorescence microscopy. J. Biol. Chem. *279*, 8403–8408.

Ohara-Imaizumi, M., Nishiwaki, C., Kikuta, T., Nagai, S., Nakamichi, Y., and Nagamatsu, S. (2004b). TIRF imaging of docking and fusion of single insulin granule motion in primary rat pancreatic beta-cells: different behaviour of granule motion between normal and Goto-Kakizaki diabetic rat beta-cells. Biochem. J. *381*, 13–18.

Ohtsuka, T., *et al.* (2002). Cast: a novel protein of the cytomatrix at the active zone of synapses that forms a ternary complex with RIM1 and Munc13-1. J. Cell Biol. *158*, 577–590.

Orci, L., Mariella, R., and Richard, G.W.A. (1987). The condensing vacuole cells is more acidic than the mature secretory vesicle. Nature *326*, 77–79.

Rizo, J., and Südhof, T. C. (2002). Snares and Munc18 in synaptic vesicle fusion. Nat. Rev. Neurosci. *8*, 641–653.

Rosenmund, C., and Sigler, A., Augustin, I., Reim, K., Brose, N., and Rhee, J. S. (2002). Differential control of vesicle priming and short-term plasticity by Munc13 isoforms. Neuron *33*, 411–424.

Rosenmund, C., Rettig, J., and Brose, N. (2003). Molecular mechanisms of active zone function. Curr. Opin. Neurobiol. *1*, 509–519.

Sadoul, K., Lang, J., Montecucco, C., Weller, U., Regazzi, R., Catsicas, S., Wollheim, C. B., and Halban, P. A. (1995). SNAP-25 is expressed in islets of Langerhans and is involved in insulin release. J. Cell Biol. *128*, 1019–1028.

Schoch, S., Castillo, P. E., Jo, T., Mukherjee, K., Geppert, M., Wang, Y., Schmitz, F., Malenka, R. C., and Südhof, T. C. (2002). RIM1α forms a protein scaffold for regulating neurotransmitter release at the active zone. Nature *415*, 321–326.

Takao-Rikitsu, E., Mochida, S., Inoue, E., Deguchi-Tawarada, M., Inoue, M., Ohtsuka, T., and Takai, Y. (2004). Physical and functional interaction of the active zone proteins, CAST, RIM1, and Bassoon, in neurotransmitter release. J. Cell Biol. *164*, 301–311.

tom Dieck, S., *et al.* (1998). Bassoon, a novel zinc-finger CAG/glutamine-repeat protein selectively localized at the active zone of presynaptic nerve terminals. J. Cell Biol. *142*, 499–509.

Vasir, B., Jonas, J. C., Steil, G. M., Hollister-Lock, J., Hasenkamp, W., Sharma, A., Bonner-Weir, S., and Weir, G. C. (2001). Gene expression of VEGF and its receptors Flk-1/KDR and Flt-1 in cultured and transplanted rat islets. Transplantation *71*, 924–935.

Wang, X., Kibschull, M., Laue, M. M., Lichte, B., Petrasch-Parwez, E., and Kilimann, M. W. (1999). Aczonin, a 550-kD putative scaffolding protein of presynaptic active zones, shares homology regions with Rim and Bassoon and binds profilin. J. Cell Biol. *147*, 151–162.

Wang, Y., Okamoto, M.,. Schmitz, F., Hofmann, K., and Südhof, T. C. (1997). Rim is a putative Rab3 effector in regulating synaptic vesicle fusion. Nature *388*, 593–598.

Wang, Y., Liu, X., Biederer, T., and Südhof, T. C. (2002). A family of RIM-binding proteins regulated by alternative splicing: implications for the genesis of synaptic active zones. Proc. Natl. Acad. Sci. USA *99*, 14464–14469.

Yokota, T., Nakata, T., Minami, S., Inazawa, J., and Emi, M. (2000). Genomic organization and chromosomal mapping of ELKS, a gene rearranged in a papillary thyroid carcinoma. J. Hum. Genet. *45*, 6–11.

Hypertension
JOURNAL OF THE AMERICAN HEART ASSOCIATION

Renin-Angiotensin System Modulates Oxidative Stress–Induced Endothelial Cell Apoptosis in Rats

Masahiro Akishita, Kumiko Nagai, Hang Xi, Wei Yu, Noriko Sudoh, Tokumitsu Watanabe, Mica Ohara-Imaizumi, Shinya Nagamatsu, Koichi Kozaki, Masatsugu Horiuchi and Kenji Toba

Hypertension 2005;45;1188-1193; originally published online May 2, 2005;
DOI: 10.1161/01.HYP.0000165308.04703.f2
Hypertension is published by the American Heart Association. 7272 Greenville Avenue, Dallas, TX 72514
 Print ISSN: 0194-911X. Online ISSN: 1524-4563

Renin-Angiotensin System Modulates Oxidative Stress–Induced Endothelial Cell Apoptosis in Rats

Masahiro Akishita, Kumiko Nagai, Hang Xi, Wei Yu, Noriko Sudoh, Tokumitsu Watanabe, Mica Ohara-Imaizumi, Shinya Nagamatsu, Koichi Kozaki, Masatsugu Horiuchi, Kenji Toba

Abstract—The role of the renin-angiotensin system in oxidative stress–induced apoptosis of endothelial cells (ECs) was investigated using a rat model and cultured ECs. EC apoptosis was induced by 5-minute intra-arterial treatment of a rat carotid artery with 0.01 mmol/L H_2O_2 and was evaluated at 24 hours by chromatin staining of *en face* specimens with Hoechst 33342. Although activity of angiotensin-converting enzyme in arterial homogenates was not increased, administration of an angiotensin-converting enzyme inhibitor temocapril for 3 days before H_2O_2 treatment inhibited EC apoptosis, followed by reduced neointimal formation 2 weeks later. Also, an angiotensin II type 1 (AT1) receptor blocker (olmesartan) inhibited EC apoptosis, whereas angiotensin II administration accelerated apoptosis independently of blood pressure. Next, cultured ECs derived from a bovine carotid artery were treated with H_2O_2 to induce apoptosis, as evaluated by DNA fragmentation. Combination of angiotensin II and H_2O_2 dose-dependently increased EC apoptosis and 8-isoprostane formation, a marker of oxidative stress. Conversely, temocapril and olmesartan reduced apoptosis and 8-isoprostane formation induced by H_2O_2, suggesting that endogenous angiotensin II interacts with H_2O_2 to elevate oxidative stress levels and EC apoptosis. Neither an AT2 receptor blocker, PD123319, affected H_2O_2-induced apoptosis, nor a NO synthase inhibitor, N^G-nitro-L-arginine methyl ester, influenced the effect of temocapril on apoptosis in cell culture experiments. These results suggest that AT1 receptor signaling augments EC apoptosis in the process of oxidative stress–induced vascular injury. (***Hypertension*. 2005;45:1188-1193.**)

Key Words: angiotensin ■ apoptosis ■ carotid arteries ■ endothelium ■ free radicals

Stress-induced injury of vascular endothelial cells (ECs) is considered to be an initial event in the development of atherosclerosis.[1] In particular, oxidative stress has been implicated in endothelial injury caused by oxidized LDL and smoking, as well as hypertension, diabetes, and ischemia reperfusion.[1–3] This notion is supported by the findings that the production of reactive oxygen species is upregulated in vascular lesions[4,5] and that lesion formation such as endothelial dysfunction is accelerated by superoxide anion[6] and, in contrast, is attenuated by free radical scavengers, including vitamin E[7] and superoxide dismutase.[8]

The renin-angiotensin system (RAS) is known to play a pivotal role in the process of vascular lesion formation such as atherosclerosis and restenosis after angioplasty. The expression of RAS components renin,[9] angiotensinogen,[10] angiotensin-converting enzyme (ACE),[11,12] and angiotensin II (Ang II) receptors[13] is upregulated in vascular lesions. Also, RAS inhibitors attenuate neointimal formation after vascular injury in animals[12,14] and endothelial dysfunction in humans.[15,16] The interaction between oxidative stress and the RAS, factors essential for the development of vascular disease, needs to be addressed. It has been demonstrated that RAS activation induces oxidative stress[17–20] and can enhance EC apoptosis in vitro.[20,21] However, it has not been elucidated whether the RAS plays a role in oxidative stress–induced vascular injury in vivo, particularly in EC apoptosis, an initial and important process in atherosclerosis.[1,22,23]

In this study, we first tested whether the RAS would augment EC apoptosis induced by brief exposure to H_2O_2 and the subsequent neointimal formation using a rat model.[24] Next, we used an in vitro model of H_2O_2-induced EC apoptosis to clarify the underlying cellular mechanism.

Methods

H_2O_2 Treatment of Carotid Artery

Ten- to 12-week-old male Wistar rats (Japan Clea; Tokyo, Japan) were used in this study. Maintenance of rats and surgical procedures for H_2O_2 treatment were performed as described previously.[24] Methods are detailed in the online data supplement (available online at http://www.hypertensionaha.org). All of the experimental protocols were approved by the animal research committee of the Kyorin University School of Medicine.

Received October 26, 2004; first decision December 13, 2004; revision accepted March 24, 2005.

From the Department of Geriatric Medicine (M.A., K.N., H.X., W.Y., N.S., K.K., K.T.), Kyorin University School of Medicine, Tokyo, Japan; Department of Geriatric Medicine (T.W.), Graduate School of Medicine, University of Tokyo, Japan; Department of Biochemistry (M.O.-I., S.N.), Kyorin University School of Medicine, Tokyo, Japan; Department of Medical Biochemistry (M.H.), Ehime University School of Medicine, Japan.

Correspondence to Masahiro Akishita, MD, PhD, Department of Geriatric Medicine, Graduate School of Medicine, The University of Tokyo, 7-3-1 Hongo, Bunkyo-ku, Tokyo 113-8655, Japan. E-mail akishita-tky@umin.ac.jp

Hypertension **is available at http://www.hypertensionaha.org** **DOI: 10.1161/01.HYP.0000165308.04703.f2**

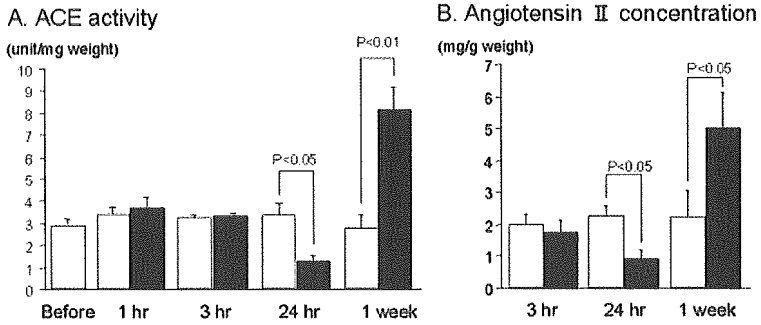

Figure 1. ACE activity and Ang II concentration in rat carotid artery after H_2O_2 treatment. Treated (closed bars) and contralateral (open bar) carotid arteries were harvested at the indicated time points after H_2O_2 treatment. ACE activity and Ang II concentration in tissue homogenates were measured using a pool of samples consisting of 6 to 10 arteries and were calibrated by the tissue wet weight. Values are expressed as mean±SEM of 5 to 6 independent pools.

Animal Groups and Blood Pressure Measurement

An ACE inhibitor, temocapril (10 mg/kg per day; donated by Sankyo Co, Ltd; Tokyo, Japan), or vehicle (40% ethanol) was administered orally using a feeding tube daily for 3 days. Separately, an Ang II type 1 (AT1) receptor blocker, olmesartan (1 mg/kg per day; donated by Sankyo Co, Ltd), or vehicle (40% ethanol) was administered orally for 3 days. Ang II was administered for 3 days using an osmotic minipump (Model 103D; Alza Corporation) prefilled with Ang II (0.7 mg/kg per day; Sigma), and implanted subcutaneously in the back. Hydralazine (25 mg/kg per day; Sigma) was orally administered alone for 5 days and subsequently with or without Ang II for 3 days before H_2O_2 treatment to abolish the effect of Ang II on blood pressure. On the last day of drug administration, blood pressure was measured with the animals in a conscious state by the tail-cuff method (BP-98A; Softron), and then H_2O_2 treatment was performed.

Measurement of ACE Activity and Ang II Concentration

At various time points after H_2O_2 treatment, the carotid arteries were dissected, weighed, and stored at −80°C. Pooled samples (n=6 to 10 for a pool) were homogenized with a polytron homogenizer in distilled water and centrifuged at 25 000*g* for 30 minutes at 4°C. ACE activity and Ang II concentration in the supernatants were measured using a colorimetric assay[12] and a sensitive radioimmunoassay, respectively. The values were calibrated by the tissue wet weight. ACE activity in the cell lysates of cultured ECs was measured using a colorimetric assay and calibrated by the protein concentration.

Evaluation of EC Apoptosis and Neointimal Formation in Carotid Artery

EC apoptosis was evaluated at 24 hours after H_2O_2 treatment as described previously.[24] Neointimal formation in the common carotid artery was evaluated 2 weeks after H_2O_2 treatment as described previously.[24] Methods are detailed in the online data supplement.

Induction of EC Apoptosis in Culture

ECs isolated from bovine carotid artery[25] were used at the fifth to seventh passage. When the cells had grown to 80% confluence, ECs were pretreated for 24 hours with culture medium containing the reagents that were tested in the experiments. Subsequently, after washing twice with Hank's balanced salt solution, the cells were exposed to H_2O_2 (0.01 to 0.2 mmol/L) diluted in Hank's balanced salt solution for 1.5 hours at 37°C to induce apoptosis. The cells were washed twice with Hank's balanced salt solution and then cultured in culture medium containing the reagents until assay.

The effects of temocapril, olmesartan, a NO synthase inhibitor, N^G-nitro-L-arginine methyl ester (L-NAME; Sigma), an Ang II type 2 (AT2) receptor blocker, PD123319 (Research Biochemical International), and Ang II (Sigma) were examined by adding them into the medium throughout the experiments.

Measurement of EC Apoptosis and Oxidative Stress Markers in Culture

For quantitative determination of apoptosis, we measured DNA fragmentation and caspase-3 activity at 24 hours after H_2O_2 treatment. DNA fragmentation was evaluated by histone-associated DNA fragments using a photometric enzyme immunoassay (EIA; Cell Death Detection ELISA; Roche) according to manufacturer instructions. Caspase-3 activity was measured using a colorimetric kit (Caspase-3 Colorimetric Activity Assay Kit; Chemicon) based on its activity to digest the substrate DVED according to manufacturer instructions.

Formation of 8-isoprostane (8-*iso* prostaglandin $F_{2\alpha}$) was measured using a commercially available EIA kit (Cayman Chemical). Culture supernatants were diluted with EIA buffer when necessary and were applied to EIA according to manufacturer instructions. Intracellular oxidative stress levels were measured using 2′,7′-dichlorofluorescein (DCF) as described previously,[26] and the intensity values were calculated using the Metamorph software.

Real-Time Polymerase Chain Reaction

Real-time polymerase chain reaction (PCR) to quantify AT1 receptor mRNA in cultured ECs was performed using SYBR Green I (Sigma) and the ABI Prism 7000 Sequence Detection System (Applied Biosystems). Methods are detailed in the online data supplement.

Data Analysis

The values are expressed as mean±SEM in the text and figure data were analyzed using 1-factor ANOVA. If a statistically significant effect was found, Newman–Keuls test was performed to isolate the difference between the groups. Differences with a value of $P<0.05$ were considered statistically significant.

Results

ACE Activity in Carotid Artery After H_2O_2 Treatment

We examined whether H_2O_2 treatment would activate ACE and stimulate Ang II synthesis in the carotid artery. As shown in Figure 1A, ACE activity in tissue homogenates was not increased at 1 to 3 hours and, rather, was decreased at 24 hours, probably because of EC denudation.[24] Low ACE activity in the de-endothelialized artery is consistent with the previous finding[11,12] and was confirmed by measurement of ACE activity in the rat carotid artery, in which ECs were denuded ex vivo using a cotton swab (data not shown). In contrast, ACE activity was significantly increased at 1 week after H_2O_2 treatment, reflecting neointimal formation.[11,12,24] Ang II concentration in arterial homogenates showed similar changes to ACE activity after H_2O_2 treatment (Figure 1B).

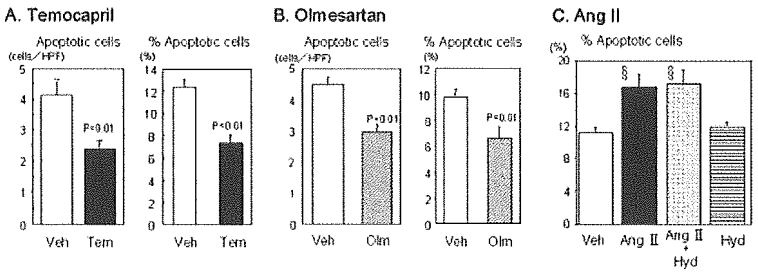

Figure 2. Effects of temocapril (A), olmesartan (B), and Ang II (C) on EC apoptosis after H_2O_2 treatment in rat carotid artery. The number of apoptotic ECs was counted per high power field (HPF; ×200), and the ratio of the apoptotic cell number to the intact cell number was calculated using *en face* specimens of the carotid artery stained with Hoechst 33342. A and B, Temocapril (Tem; 10 mg/kg per day; n=12), olmesartan (Olm; 1 mg/kg per day; n=8), or their vehicle (Veh; n=10 and n=6, respectively) was administered orally for 3 days before H_2O_2 treatment. C, Ang II (0.7 mg/kg per day) or its vehicle was administered subcutaneously for 3 days using an osmotic minipump alone (n=8 for Ang II and n=10 for vehicle) or in combination with oral administration of hydralazine (Hyd; 25 mg/kg per day; n=6 for Ang II and n=6 for vehicle; single administration for 5 days and coadministration with Ang II for 3 days) before H_2O_2 treatment. §$P<0.01$ vs vehicle. Values are expressed as mean±SEM.

Effect of RAS Inhibitors and Ang II on EC Apoptosis After H_2O_2 Treatment in Rats

The effects of an ACE inhibitor, temocapril, and an AT1 receptor blocker, olmesartan, on EC apoptosis were examined at 24 hours after H_2O_2 treatment because the peak of apoptosis was observed at 6 to 24 hours.[24] Administration of 10 mg/kg per day temocapril or 1 mg/kg per day olmesartan for 3 days before H_2O_2 treatment did not significantly change body weight, heart rate, or blood pressure, but this dose of temocapril effectively inhibited plasma ACE activity (data not shown). The number and percentage of apoptotic cells, as determined using *en face* specimens with Hoechst 33342 staining, were significantly decreased by temocapril compared with vehicle (Figure 2A; supplemental Figure I, available online at http://www.hypertensionaha.org). Olmesartan showed a comparable inhibitory effect on EC apoptosis (Figure 2B).

Ang II was administered for 3 days in combination with hydralazine to eliminate the effect of Ang II on blood pressure. Consequently, systolic blood pressure was higher in rats administered Ang II alone (161±5 mm Hg; $P<0.01$) than in the other groups of rats: 123±3 mm Hg in the vehicle group, 129±7 mm Hg in the Ang II plus hydralazine group, and 114±4 mm Hg in the hydralazine group. In contrast to RAS inhibitors, Ang II administration augmented EC apoptosis independent of the pressor effect because coadministration of hydralazine did not influence EC apoptosis (Figure 2C).

Inhibitory Effect of Temocapril on Neointimal Formation

We examined whether inhibition of EC apoptosis by temocapril would result in a reduction of neointimal formation. To do so, histological analysis of the carotid artery was performed 2 weeks after H_2O_2 treatment. Temocapril significantly decreased the neointimal area and the intima/media area ratio: intima/media area ratio was 0.18±0.02 in the vehicle group versus 0.12±0.02 in the temocapril group (n=9; $P<0.05$; supplemental Figure II). Because temocapril was administered for only 3 days before H_2O_2 treatment, it is suggested that inhibition of EC apoptosis may play a mechanistic role in attenuation of neointimal formation, although ACE inhibitors have various effects such as anti-inflammation and antimigration as well.

Effect of RAS Inhibitors on H_2O_2-Induced EC Apoptosis in Culture

To reproduce oxidative stress–induced EC apoptosis in culture, we applied 0.2 mmol/L H_2O_2 to cultured ECs derived from a bovine carotid artery for 1.5 hours based on dose- and time-response experiments. EC apoptosis, as determined by DNA fragmentation and caspase-3 activity, was induced at 24 hours after H_2O_2 treatment. Comparable to in vivo experiments, temocapril inhibited EC apoptosis in a dose-dependent manner (Figure 3A and 3B). The inhibitory effect on EC apoptosis was mimicked by 10 μmol/L olmesartan (Figure 3C), but an AT2 receptor blocker, PD123319, did not influence EC apoptosis (supplemental Figure IIIA). The involvement of NO in the effect of temocapril was examined using an NO synthase inhibitor, L-NAME, because ACE inhibitors stimulate NO production via the inhibition of bradykinin degradation.[12] However, L-NAME did not influence the effect of temocapril (supplemental Figure IIIB).

To make the interaction between H_2O_2 and Ang II clear, dose response and combined effects of both agents on EC apoptosis and 8-isoprostane formation, a marker of oxidative stress, were examined. As shown in Figures 3D and 4A, combination of Ang II and H_2O_2 dose-dependently stimulated EC apoptosis and 8-isoprostane formation. Conversely, temocapril and olmesartan restrained 8-isoprostane formation (Figure 4B) and intracellular DCF formation (Figure 4C; supplemental Figure IV) induced by H_2O_2, suggesting that endogenous Ang II also interacts with H_2O_2 to elevate oxidative stress levels.

ACE activity and the expression of AT1 receptor mRNA in cultured ECs were determined. ACE activity calibrated by the protein concentration was not changed after H_2O_2 treatment: 106±9% at 3 hours and 103±8% at 24 hours after H_2O_2 treatment compared with the values at baseline and 3 hours after vehicle treatment (100±3% and 96±13%, respectively; n=3). The relative amount of the AT1 receptor to the housekeeping gene G3PDH, as measured by real-time PCR analysis, was not significantly changed after H_2O_2 treatment: 91±2% at 1.5 hours during the treatment, 99±5% at 3 hours, and 102±4% at 6 hours after H_2O_2 treatment compared with vehicle treatment (100±6%; n=3). Considering negative regulation in vascular smooth muscle cells[27,28] together, upregulation of the AT1 receptor is not likely to occur in response to H_2O_2 treatment.

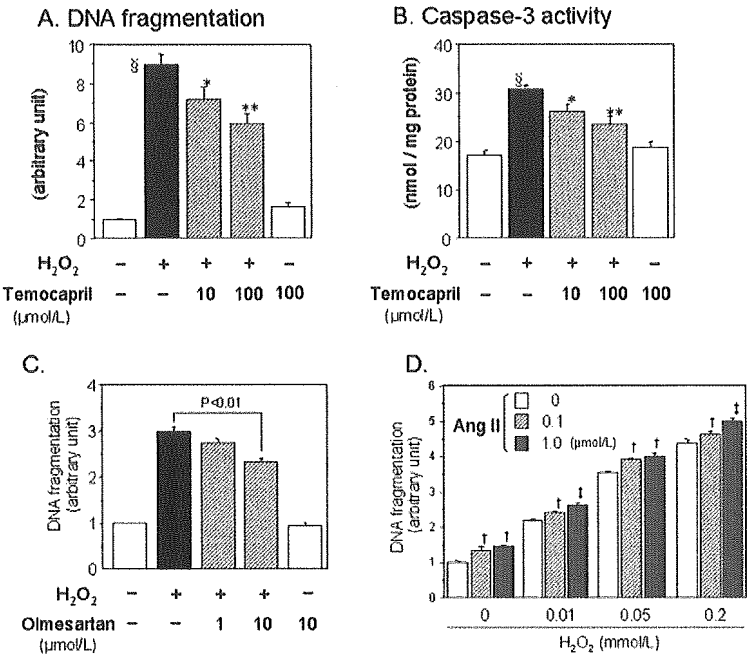

Figure 3. Effects of temocapril (A and B), olmesartan (C), and Ang II (D) on H_2O_2-induced EC apoptosis in culture. A through D, Temocapril, olmesartan, Ang II, or their vehicle was added to the culture medium 24 hours before H_2O_2 treatment until assay. EC apoptosis was evaluated 24 hours after H_2O_2 treatment (0.2 mmol/L in A through C; 0.01 to 0.2 mmol/L in D) by means of DNA fragmentation (A, C, and D; n=3) and caspase-3 activity (B; n=4). §$P<0.01$ vs H_2O_2 (−). *$P<0.05$; **$P<0.01$ vs H_2O_2 (+) + temocapril (−). †$P<0.05$ vs Ang II (−). ‡$P<0.05$ vs Ang II 0.1 μmol/L. Values are expressed as mean±SEM. Similar results were obtained in 3 independent experiments.

Discussion

This study was conducted to elucidate the role of the RAS in oxidative stress–induced EC apoptosis using a rat model and cultured ECs. Treatment with H_2O_2 did not increase ACE activity or Ang II in the rat carotid artery during the acute phase. However, administration of an ACE inhibitor, temocapril, and an AT1 receptor blocker, olmesartan, inhibited EC apoptosis in vivo. Furthermore, we demonstrated using cultured ECs that combination of Ang II and H_2O_2 dose-dependently increased EC apoptosis and 8-isoprostane formation. In addition, temocapril and olmesartan reduced but not canceled EC apoptosis and 8-isoprostane formation induced by H_2O_2, suggesting that endogenous Ang II interacts with H_2O_2 to elevate oxidative stress levels and EC apoptosis.

In vascular lesions such as atherosclerosis and intimal hyperplasia, the production of reactive oxygen species[4,5] as well as the components of the RAS[9–12] are upregulated, suggesting a possible interaction between them. A number of investigations have clarified that Ang II induces oxidative stress in vascular cells. Ang II stimulates the production of reactive oxygen species in ECs by upregulating the subunits of NAD(P)H oxidase: gp91 phox[17] and p47 phox.[18] It has been reported that the RAS enhances EC apoptosis in vitro[20,21] and contributes to endothelial dysfunction in patients with renovascular hypertension through the oxidant-dependent mechanism.[19] Conversely, it remains unknown whether oxidative stress could regulate the RAS; only 1 report has shown the modulation of ACE by oxidative stress.[29] Usui et al[29] reported that the inhibition of NO synthesis by chronic administration of L-NAME in rats augmented superoxide production and ACE activity in aortic ECs, and these effects were eliminated by treatment with

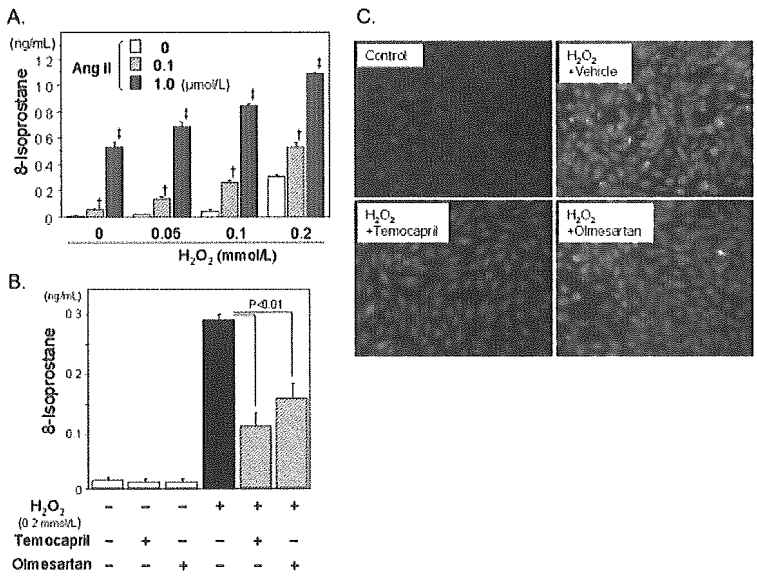

Figure 4. Effects of Ang II (A), temocapril, and olmesartan (B and C) on 8-isoprostane and DCF formation in cultured ECs. Ang II, temocapril (100 μmol/L), olmesartan (10 μmol/L), or their vehicle was added to the culture medium 24 hours before H_2O_2 treatment until assay. Then 8-isoprostane concentration in the culture supernatant and intracellular DCF intensity were measured 3 hours after H_2O_2 treatment. †$P<0.05$ vs Ang II (−). ‡$P<0.05$ vs Ang II 0.1 μmol/L. Values are expressed as mean±SEM (n=3). Similar results were obtained in 3 independent experiments.

antioxidants. In the present study, ACE activity in the carotid artery was not increased until 24 hours after H_2O_2 treatment. We also found that ACE activity was not changed after H_2O_2 treatment in cell culture experiments. Furthermore, the expression of AT1 receptor mRNA in cultured ECs, as measured using real-time PCR, was not increased after H_2O_2 treatment. Together, it is not likely that Ang II production or its receptor expression was upregulated in response to H_2O_2.

However, an ACE inhibitor, temocapril, and an AT1 receptor blocker, olmesartan, inhibited H_2O_2-induced EC apoptosis in rats as well as in cell culture experiments. No influence of L-NAME on the antiapoptotic effect of temocapril in cell culture studies indicates that the effect of temocapril was attributable to the inhibition of Ang II synthesis. An AT2 receptor blocker, PD123319, did not influence H_2O_2-induced EC apoptosis either. This result appears to be inconsistent with the previous finding[30] but suggests a minimal contribution of the AT2 receptor in H_2O_2-induced EC apoptosis or minimal expression of the AT2 receptor in the cultured ECs used in the present study. Reduction in 8-isoprostane formation by temocapril and olmesartan suggests that endogenous Ang II adds to the oxidative stress levels on top of exogenous H_2O_2; otherwise temocapril and olmesartan would have antioxidant effects independent of Ang II through currently unknown mechanisms, although the in vivo role of bradykinin/NO in the effect of ACE inhibitors and that of the AT2 receptor remain to be addressed.

Administration of Ang II provided evidence that Ang II can interact with H_2O_2 to elevate oxidative stress levels and induce EC apoptosis. In rat experiments, a high and pressor dose of Ang II was used in combination with hydralazine[31] because 3-day administration of lower doses of Ang II (0.1 to 0.2 mg/kg per day) did not show significant effects on EC apoptosis (data not shown). The cell culture experiments to examine the effect of submaximal doses of Ang II and H_2O_2 on apoptosis and 8-isoprostane formation gave us clear information that AT1 receptor signaling augments EC apoptosis by an interaction with oxidative stress. Although the doses of H_2O_2 and the time duration of exposure were optimized on the basis of the time- and dose-response experiments, the conditions in cell culture studies were different from those in animal studies. However, it has been reported that cigarette smoke, oxidized lipoproteins, and polymorphonuclear leukocytes, which play important roles in atherogenesis, can generate H_2O_2 concentrations of 0.05 to 0.2 mmol/L in vitro.[32] These reports suggest that the dosages of H_2O_2 used in the present study do not far exceed the physiological range, although direct comparison of physiological or pathophysiological conditions with those in our experiments may be inappropriate.

Considering the stimulatory effect of Ang II on free radical production,[17–19] our finding that endogenous Ang II exacerbates EC apoptosis induced by exogenous H_2O_2 is not surprising. In fact, a number of reports have shown experimentally that RAS inhibitors can reduce the production of reactive oxygen species in pathological conditions such as peripheral arteries in rats with chronic heart failure,[33] rat diabetic nephropathy,[34] and kidney mitochondria in aged rats.[35] In the clinical setting, it is reported that administration of an AT1 receptor blocker (losartan) to patients with chronic renal disease reduced urinary excretion of oxidized albumin and malondialdehyde.[36] Also, 4-week treatment with losartan or an ACE inhibitor (ramipril) in patients with coronary artery disease diminished the response of endothelium-dependent vasodilation to intracoronary administration of antioxidant vitamin C in parallel with improvement of basal endothelium-dependent vasodilation,[37] indicating that RAS inhibitors can improve endothelial function in association with a reduction of oxidative stress. In the present study, we investigated EC apoptosis, an important process that leads to endothelial dysfunction and atherosclerosis[22,23] using an in vivo model. Moreover, our finding that RAS inhibitors attenuated EC apoptosis suggests broad end-organ protective effects of RAS inhibitors, which have been used for the treatment of hypertension and heart failure.

Perspectives

We found using an in vivo model and cultured ECs that Ang II elevated oxidative stress levels and increased EC apoptosis, whereas RAS inhibitors restrained them. These findings will add new information for cardiovascular research and the clinical application of RAS inhibitors.

Acknowledgments

This study was supported by a grant-in-aid for scientific research from the Ministry of Education, Science, Culture and Sports of Japan (13670741), and by Health and Labor Sciences Research Grants (H15-Choju-013 and H15-Choju-015) from the Ministry of Health, Labor and Welfare of Japan. We thank Mariko Sawano for her excellent technical assistance.

References

1. Ross R. Atherosclerosis–an inflammatory disease. *N Engl J Med.* 1999; 340:115–126.
2. Griendling KK, Sorescu D, Lassegue B, Ushio-Fukai M. Modulation of protein kinase activity and gene expression by reactive oxygen species and their role in vascular physiology and pathophysiology. *Arterioscler Thromb Vasc Biol.* 2000;20:2175–2183.
3. Zalba G, San Jose G, Moreno MU, Fortuno MA, Fortuno A, Beaumont FJ, Diez J. Oxidative stress in arterial hypertension: role of NAD(P)H oxidase. *Hypertension.* 2001;38:1395–1399.
4. Sorescu D, Weiss D, Lassegue B, Clempus RE, Szocs K, Sorescu GP, Valppu L, Quinn MT, Lambeth JD, Vega JD, Taylor WR, Griendling KK. Superoxide production and expression of nox family proteins in human atherosclerosis. *Circulation.* 2002;105:1429–1435.
5. Spiekermann S, Landmesser U, Dikalov S, Bredt M, Gamez G, Tatge H, Reepschlager N, Hornig B, Drexler H, Harrison DG. Electron spin resonance characterization of vascular xanthine and NAD(P)H oxidase activity in patients with coronary artery disease: relation to endothelium-dependent vasodilation. *Circulation.* 2003;107:1383–1389.
6. Rey FE, Li XC, Carretero OA, Garvin JL, Pagano PJ. Perivascular superoxide anion contributes to impairment of endothelium-dependent relaxation: role of gp91(phox). *Circulation.* 2002;106:2497–2502.
7. Pratico D, Tangirala RK, Rader DJ, Rokach J, FitzGerald GA. Vitamin E suppresses isoprostane generation in vivo and reduces atherosclerosis in ApoE-deficient mice. *Nat Med.* 1998;4:1189–1192.
8. Fennell JP, Brosnan MJ, Frater AJ, Hamilton CA, Alexander MY, Nicklin SA, Heistad DD, Baker AH, Dominiczak AF. Adenovirus-mediated overexpression of extracellular superoxide dismutase improves endothelial dysfunction in a rat model of hypertension. *Gene Ther.* 2002;9:110–117.
9. Iwai N, Izumi M, Inagami T, Kinoshita M. Induction of renin in medial smooth muscle cells by balloon injury. *Hypertension.* 1997;29: 1044–1050.
10. Rakugi H, Jacob HJ, Krieger JE, Ingelfinger JR, Pratt RE. Vascular injury induces angiotensinogen gene expression in the media and neointima. *Circulation.* 1993;87:283–290.

11. Rakugi H, Kim DK, Krieger JE, Wang DS, Dzau VJ, Pratt RE. Induction of angiotensin converting enzyme in the neointima after vascular injury. Possible role in restenosis. *J Clin Invest*. 1994;93:339–346.
12. Akishita M, Shirakami G, Iwai M, Wu L, Aoki M, Zhang L, Toba K, Horiuchi M. Angiotensin converting enzyme inhibitor restrains inflammation-induced vascular injury in mice. *J Hypertens*. 2001;19: 1083–1088.
13. Akishita M, Horiuchi M, Yamada H, Zhang L, Shirakami G, Tamura K, Ouchi Y, Dzau VJ. Inflammation influences vascular remodeling through AT2 receptor expression and signaling. *Physiol Genomics*. 2000;2:13–20.
14. Wu L, Iwai M, Nakagami H, Li Z, Chen R, Suzuki J, Akishita M, de Gasparo M, Horiuchi M. Roles of angiotensin II type 2 receptor stimulation associated with selective angiotensin II type 1 receptor blockade with valsartan in the improvement of inflammation-induced vascular injury. *Circulation*. 2001;104:2716–2721.
15. Antony I, Lerebours G, Nitenberg A. Angiotensin-converting enzyme inhibition restores flow-dependent and cold pressor test-induced dilations in coronary arteries of hypertensive patients. *Circulation*. 1996;94: 3115–3122.
16. Prasad A, Tupas-Habib T, Schenke WH, Mincemoyer R, Panza JA, Waclawin MA, Ellahham S, Quyyumi AA. Acute and chronic angiotensin-1 receptor antagonism reverses endothelial dysfunction in atherosclerosis. *Circulation*. 2000;101:2349–2354.
17. Rueckschloss U, Quinn MT, Holtz J, Morawietz H. Dose-dependent regulation of NAD(P)H oxidase expression by angiotensin II in human endothelial cells: protective effect of angiotensin II type 1 receptor blockade in patients with coronary artery disease. *Arterioscler Thromb Vasc Biol*. 2002;22:1845–1851.
18. Landmesser U, Cai H, Dikalov S, McCann L, Hwang J, Jo H, Holland SM, Harrison DG. Role of p47(phox) in vascular oxidative stress and hypertension caused by angiotensin II. *Hypertension*. 2002;40:511–515.
19. Higashi Y, Sasaki S, Nakagawa K, Matsuura H, Oshima T, Chayama K. Endothelial function and oxidative stress in renovascular hypertension. *N Engl J Med*. 2002;346:1954–1962.
20. Dimmeler S, Zeiher AM. Reactive oxygen species and vascular cell apoptosis in response to angiotensin II and pro-atherosclerotic factors. *Regul Pept*. 2000;90:19–25.
21. Lin LY, Lin CY, Su TC, Liau CS. Angiotensin II-induced apoptosis in human endothelial cells is inhibited by adiponectin through restoration of the association between endothelial nitric oxide synthase and heat shock protein 90. *FEBS Lett*. 2004;574:106–110.
22. Choy JC, Granville DJ, Hunt DW, McManus BM. Endothelial cell apoptosis: biochemical characteristics and potential implications for atherosclerosis. *J Mol Cell Cardiol*. 2001;33:1673–1690.
23. Dimmeler S, Haendeler J, Zeiher AM. Regulation of endothelial cell apoptosis in atherothrombosis. *Curr Opin Lipidol*. 2002;13:531–536.
24. Sudoh N, Toba K, Akishita M, Ako J, Hashimoto M, Iijima K, Kim S, Liang YQ, Ohike Y, Watanabe T, Yamazaki I, Yoshizumi M, Eto M, Ouchi Y. Estrogen prevents oxidative stress-induced endothelial cell apoptosis in rats. *Circulation*. 2001;103:724–729.
25. Akishita M, Kozaki K, Eto M, Yoshizumi M, Ishikawa M, Toba K, Orimo H, Ouchi Y. Estrogen attenuates endothelin-1 production by bovine endothelial cells via estrogen receptor. *Biochem Biophys Res Commun*. 1998;251:17–21.
26. Tampo Y, Kotamraju S, Chitambar CR, Kalivendi SV, Keszler A, Joseph J, Kalyanaraman B. Oxidative stress-induced iron signaling is responsible for peroxide-dependent oxidation of dichlorodihydrofluorescein in endothelial cells: role of transferrin receptor-dependent iron uptake in apoptosis. *Circ Res*. 2003;92:56–63.
27. Nickenig G, Strehlow K, Baumer AT, Baudler S, Wassmann S, Sauer H, Bohm M. Negative feedback regulation of reactive oxygen species on AT1 receptor gene expression. *Br J Pharmacol*. 2000;131:795–803.
28. Ichiki T, Takeda K, Tokunou T, Funakoshi Y, Ito K, Iino N, Takeshita A. Reactive oxygen species-mediated homologous downregulation of angiotensin II type 1 receptor mRNA by angiotensin II. *Hypertension*. 2001; 37:535–540.
29. Usui M, Egashira K, Kitamoto S, Koyanagi M, Katoh M, Kataoka C, Shimokawa H, Takeshita A. Pathogenic role of oxidative stress in vascular angiotensin-converting enzyme activation in long-term blockade of nitric oxide synthesis in rats. *Hypertension*. 1999;34:546–551.
30. Dimmeler S, Rippmann V, Weiland U, Haendeler J, Zeiher AM. Angiotensin II induces apoptosis of human endothelial cells. Protective effect of nitric oxide. *Circ Res*. 1997;81:970–976.
31. Fukui T, Ishizaka N, Rajagopalan S, Laursen JB, Capers Q 4th, Taylor WR, Harrison DG, de Leon H, Wilcox JN, Griendling KK. p22phox mRNA expression and NADPH oxidase activity are increased in aortas from hypertensive rats. *Circ Res*. 1997;80:45–51.
32. De Bono DP. Free radicals and antioxidants in vascular biology: the roles of reaction kinetics, environment and substrate turnover. *QJM*. 1994;87: 445–453.
33. Varin R, Mulder P, Tamion F, Richard V, Henry JP, Lallemand F, Lerebours G, Thuillez C. Improvement of endothelial function by chronic angiotensin-converting enzyme inhibition in heart failure: role of nitric oxide, prostanoids, oxidant stress, and bradykinin. *Circulation*. 2000;102: 351–356.
34. Onozato ML, Tojo A, Goto A, Fujita T, Wilcox CS. Oxidative stress and nitric oxide synthase in rat diabetic nephropathy: effects of ACEI and ARB. *Kidney Int*. 2002;61:186–194.
35. de Cavanagh EM, Piotrkowski B, Basso N, Stella I, Inserra F, Ferder L, Fraga CG. Enalapril and losartan attenuate mitochondrial dysfunction in aged rats. *FASEB J*. 2003;17:1096–1098.
36. Agarwal R. Proinflammatory effects of oxidative stress in chronic kidney disease: role of additional angiotensin II blockade. *Am J Physiol Renal Physiol*. 2003;284:F863–F869.
37. Hornig B, Landmesser U, Kohler C, Ahlersmann D, Spiekermann S, Christoph A, Tatge H, Drexler H. Comparative effect of ace inhibition and angiotensin II type 1 receptor antagonism on bioavailability of nitric oxide in patients with coronary artery disease: role of superoxide dismutase. *Circulation*. 2001;103:799–805.